

# Шнобелевская премия (Ig Nobel Prize)

— как гласит всемогущая википедия, Шно́белевская (Игнобелевская[1], Антинобелевская[1]) премия (англ. Ig Nobel Prize, от игры слов: англ. ignoble — «постыдный») — пародия на престижную международную награду — Нобелевскую премию. Десять Шнобелевских премий вручаются в начале октября, то есть в то время, когда называются лауреаты настоящей Нобелевской премии, — «за достижения, которые заставляют сначала засмеяться, а потом — задуматься» (first make people laugh, and then make them think). Премия учреждена Марком Абрахамсом и юмористическим журналом «Анналы невероятных исследований» в 1991 году



Marc Abrahams



Ig Nobel Prize Winner Dr. Elena Bodnar demonstrates her invention (a brassiere that can quickly convert into a pair of protective face masks) assisted by Nobel laureates Wolfgang Ketterle (left), Orhan Pamuk, and Paul Krugman (right). Photo credit: Alexey Eliseev, 2009 Ig Nobel Ceremony

ВОЗМОЖНЫЕ  
НОМИНАНТЫ

# Метод определения степени разбавления виски на основе изучения следов, оставшихся после высыхания капель

ACS NANO

www.acsnano.org

## Multiscale Self-Assembly of Distinctive Weblike Structures from Evaporated Drops of Dilute American Whiskeys

Adam D. Carrithers,<sup>§</sup> Martin J. Brown, VI,<sup>§</sup> Mohamed Z. Rashed, Sabina Islam, Orfin D. Velez, and Stuart J. Williams\*

Cite This: <https://dx.doi.org/10.1021/acsnano.9b08984>

Read Online

ACCESS | Metrics & More | Article Recommendations | Supporting Information



**ABSTRACT:** When a sessile droplet of a complex mixture evaporates, its nonvolatile components may deposit into various patterns. One such phenomena, the coffee ring effect, has been a topic of interest for several decades. Here, we identify what we believe to be a fascinating phenomenon of droplet pattern deposition for another well-known beverage—what we have termed a “whiskey web”. Nanoscale agglomerates were generated in diluted American whiskeys (20–25% alcohol by volume), which later stratified as microwebs on the liquid–air interface during evaporation. The web’s strandlike features result from monolayer collapse, and the resulting pattern is a function of the intrinsic molecular constituents of the whiskey. Data suggest that, for our conditions (diluted 1.0  $\mu\text{L}$  drops evaporated on cleaned glass substrates), whiskey webs were unique to diluted American whiskey; however, similar structures were generated with other whiskeys under different conditions. Further, each product forms their own distinct pattern, demonstrating that this phenomenon could be used for sample analysis and counterfeit identification.

**KEYWORDS:** self-assembly, colloids, surface monolayers, Marangoni flow, droplet evaporation, whiskey

An evaporating droplet containing nonvolatile solutes leaves a deposit whose form is dependent on the intrinsic properties of the liquid,<sup>1,2</sup> the nature of the solutes or particles,<sup>3,4</sup> and the environmental conditions under which evaporation takes place.<sup>5,6</sup> Understanding the deposition of such nonvolatile solutes is critical for engineering of coating and patterning processes.<sup>7</sup> One common phenomenon, which can arise in these coating processes, is the coffee ring deposition effect where solute particles are transported to the pinned contact line via capillary flow.<sup>8</sup> Suppression of the coffee ring effect has been extensively studied with various liquids,<sup>9</sup> including Scotch whiskey, which yielded nearly uniform particle deposition.<sup>10</sup>

Here, we demonstrate a self-assembled structure resulting from the evaporation of a volatile sessile drop of American whiskeys—depositing hierarchical weblike patterns that we have termed a “whiskey web”.<sup>11</sup> These webbed patterns were formed by evaporating a 1.0  $\mu\text{L}$  droplet of diluted American whiskey onto a clean glass coverslip. Results herein will

Received: November 12, 2019

Accepted: March 9, 2020

ARTICLE

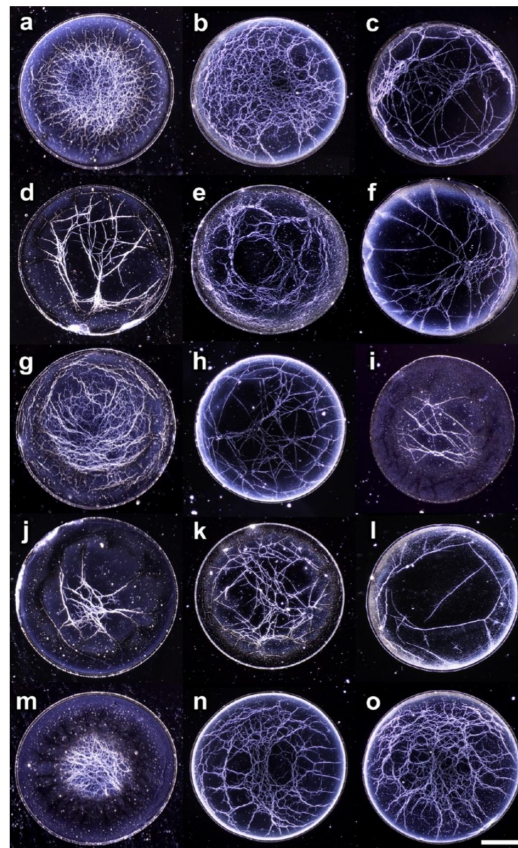


Figure 1. Examples of the surprisingly diverse “whiskey web” patterns. The patterns, approximately 2 mm in diameter, were formed by drying droplets from various off-the-shelf whiskey products diluted to 20–25% alcohol by volume. Scale bar is 0.5 mm. Refer to Table S1 in the Supporting Information for sample identification. Adapted with permission under a Creative Commons Attribution-NonCommercial 4.0 International License from ref 11, <https://doi.org/10.1103/APS.DFD.2018.GFM.P0002>. Copyright 2018 Stuart J. Williams.



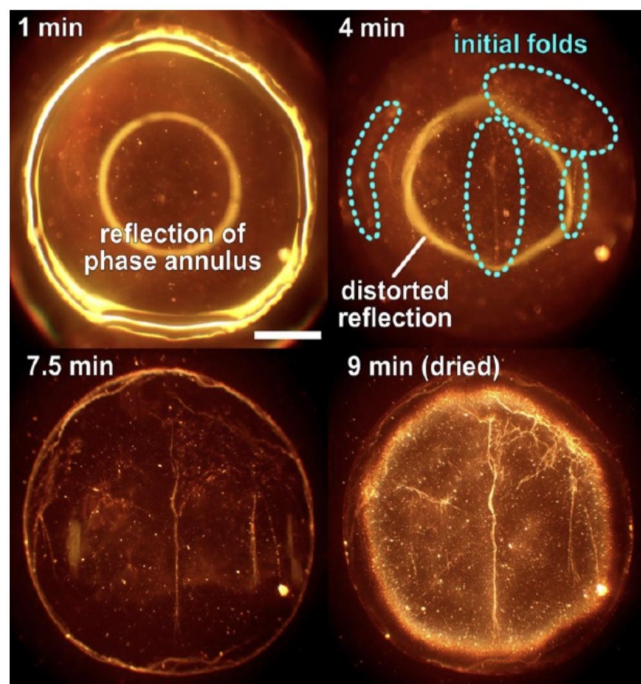


Figure 3. Time-lapse of a  $0.75\ \mu\text{L}$  drop of diluted (25% ABV) bourbon whiskey evaporating on the surface of an ITO-coated glass slide under ambient conditions. Evaporation is observed with an upright microscope using a dark-field phase annulus. At 4 min, monolayer folds were observed that subsequently impact the topography of the droplet. Additional folds were created as the droplet evaporates (7.5 min), and these features are highlighted once the liquid has completely evaporated (9 min). Scale bar is 0.5 mm

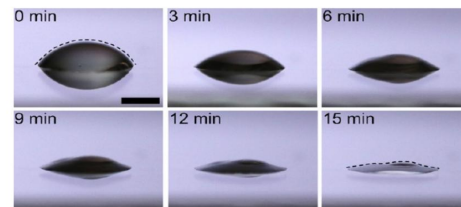


Figure 4. Series of images illustrating the evaporation of  $2.5\ \mu\text{L}$  drop of diluted (25% ABV) bourbon whiskey on the surface of an ITO-coated glass slide under ambient conditions. A distorted (*i.e.*, nonaxisymmetric) surface profile is observed, suggesting inhomogeneous mechanical properties at the liquid–air interface. Scale bar is 1.0 mm. Refer to Table S1 in the Supporting Information for sample identification.

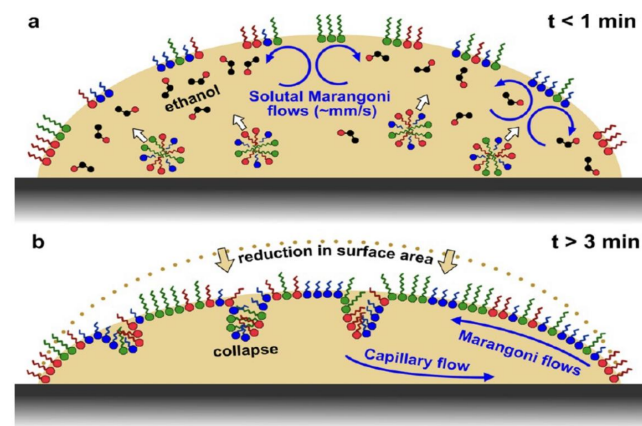


Figure 5. Schematic of the two general phases of flow and monolayer self-assembly observed during whiskey web assembly. (a) First phase is characterized by erratic solutal Marangoni vortices as ethanol is driven to the liquid–air interface, influencing monolayer formation and composition. (b) Monolayer collapse occurs during bulk evaporation as the interfacial area of the droplet decreases and was first observed approximately 3 min into droplet evaporation. Significantly reduced radial flows were observed.

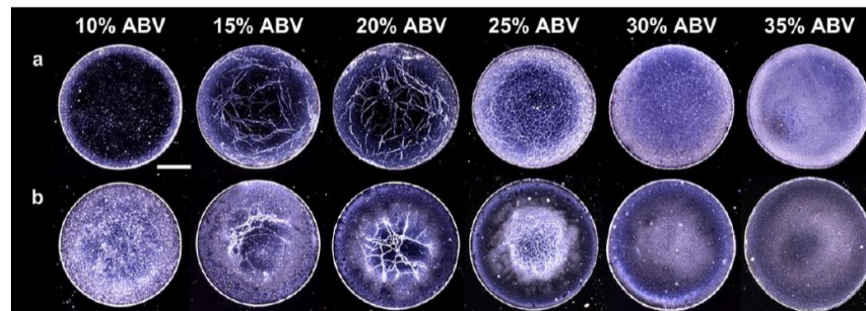


Figure 7. Effect of dilution on the deposited whiskey webs. Web formation of various aged samples: (a) 3 years old and (b) 23 years old. Scale bar is 0.5 mm. Refer to [Table S1](#) in the Supporting Information for sample identification.

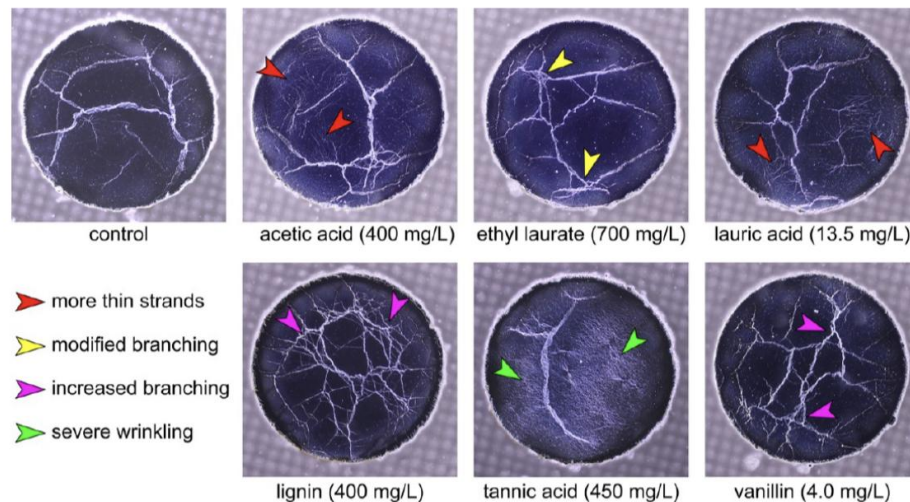


Figure 8. Effect of a set of model congeners on whiskey web patterns. Various congeners were added to a control bourbon whiskey to demonstrate that the concentration and combination of these compounds ultimately guide each whiskey web pattern.

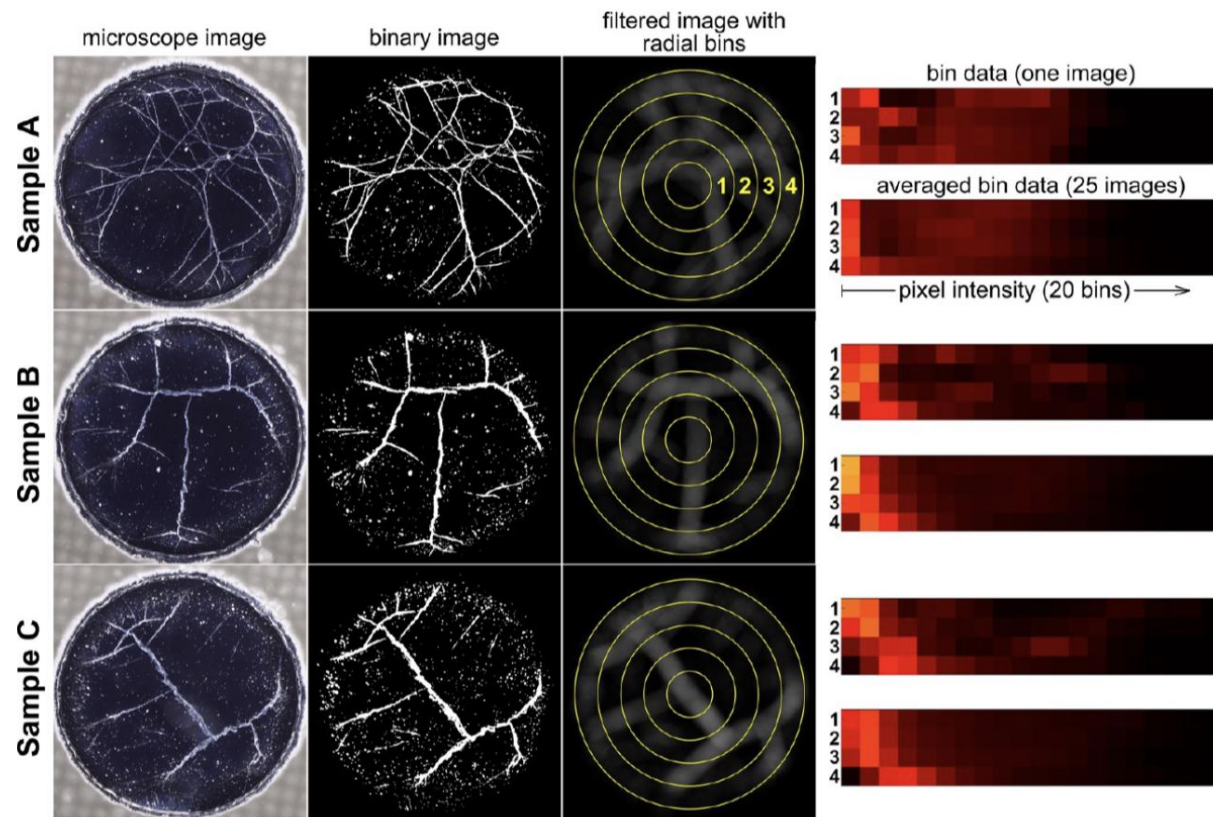


Figure 9. Analysis of microscope images of web patterns. Thirty droplets of each tested American whiskey sample were imaged and analyzed. Digital images were converted to binary images and processed with a radial filter. Each pixel was then placed into a bin based on their radial position (four bins) and intensity (20 bins). Twenty-five arrays were averaged to represent a given American whiskey sample. The remaining 15 droplets (five of each sample) were tested against the averaged representative data. A single image was matched with its American whiskey over 90% of the time. Refer to [Table S1](#) in the Supporting Information for sample identification.

# Изучение характерных свойств аромата выдержанного коньяка по сравнению с молодым

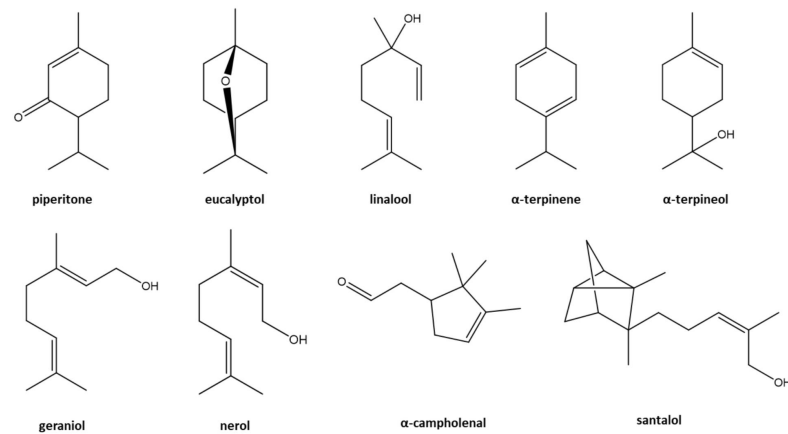
Journal of Agricultural and Food Chemistry

## Contribution of Volatile Odorous Terpenoid Compounds to Aged Cognac Spirits Aroma in a Context of Multicomponent Odor Mixtures.

Fannie Thibaud,<sup>†</sup> Marie Courregelongue,<sup>†</sup> and Philippe Darriet<sup>†</sup>

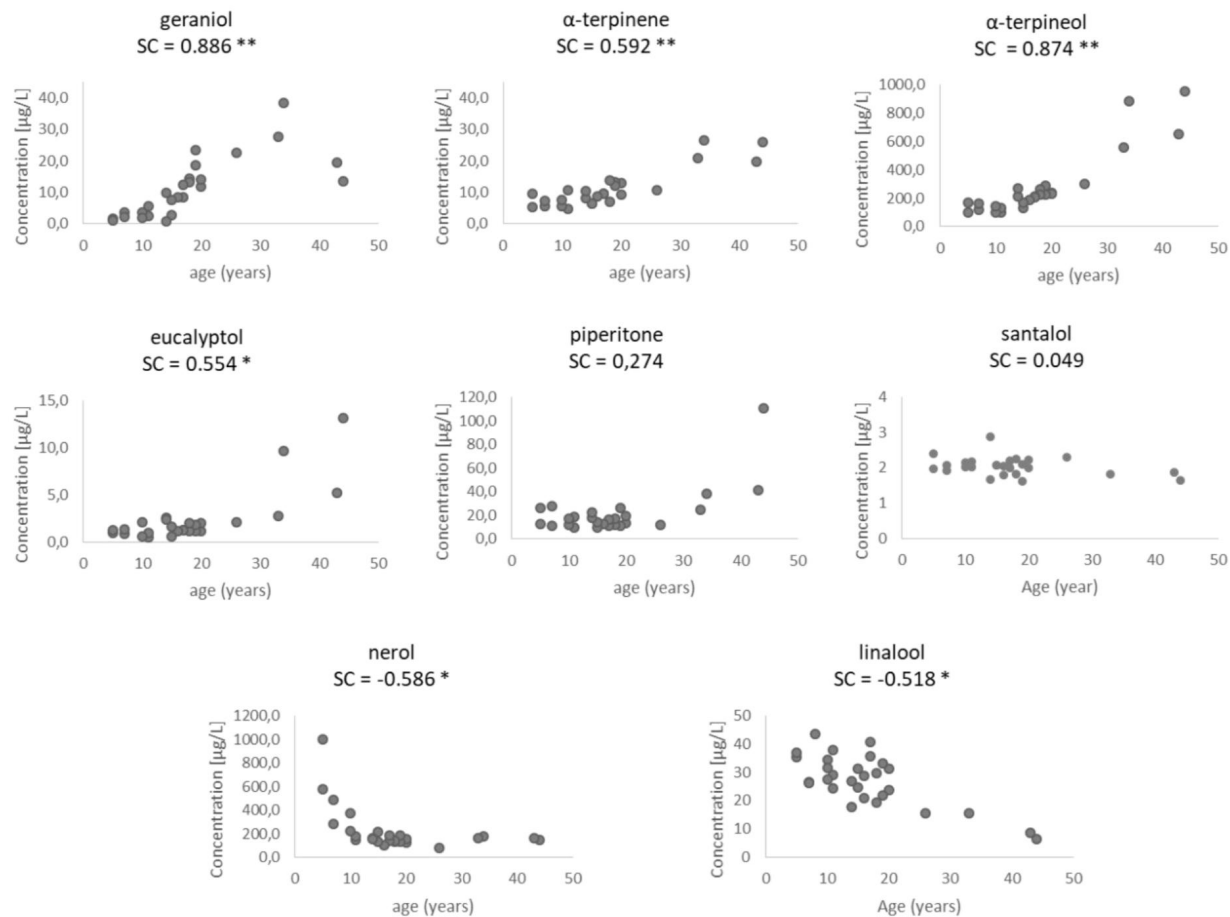
<sup>†</sup> Univ. Bordeaux, Unité de recherche Œnologie, EA 4577, USC 1366 INRA, ISVV, 33882  
Villenave d'Ornon cedex, France

Figure 1:

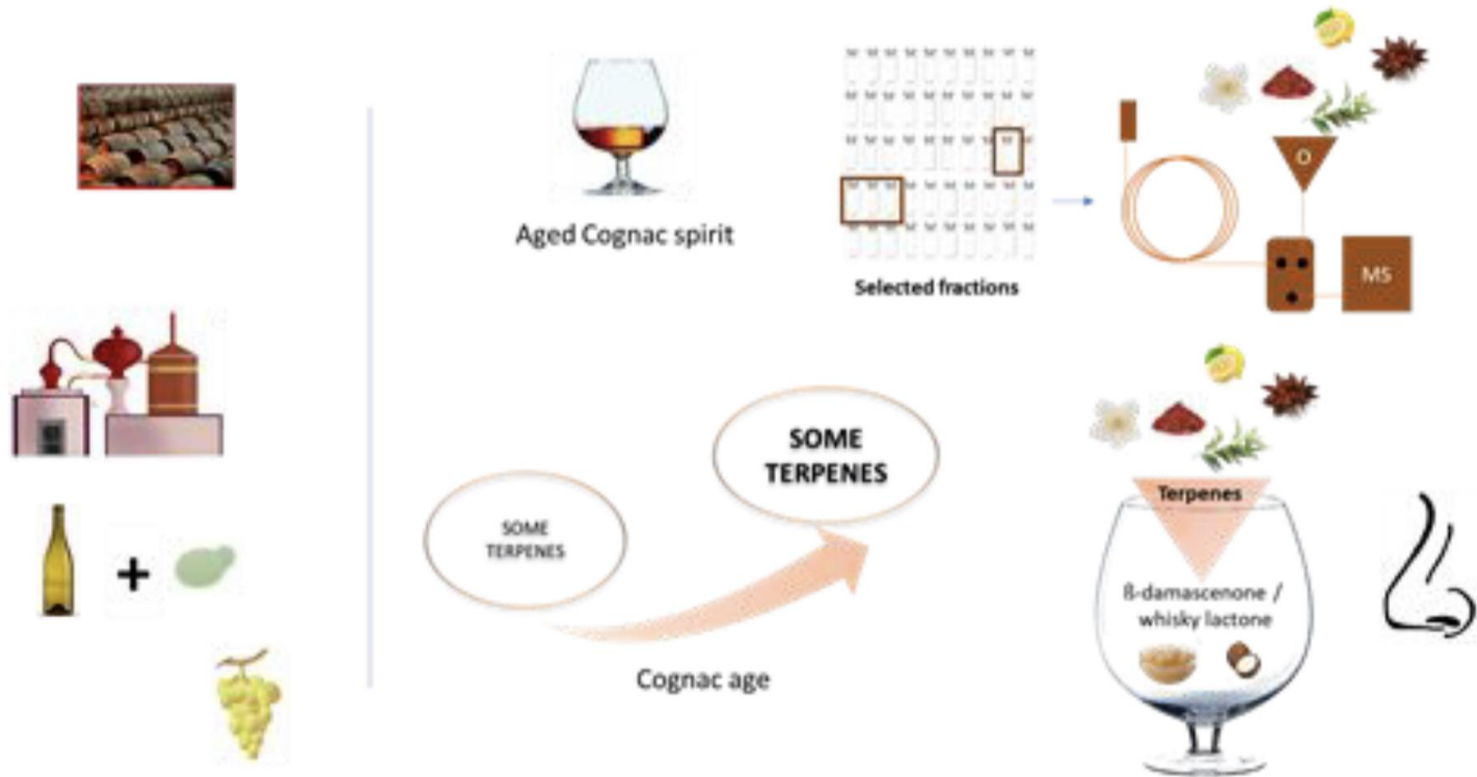




**Figure 2:**



# For Table of Contents Only



# Темнота помогла самцам дрозофил пережить моральную травму от неудачных ухаживаний

## Environmental light is required for maintenance of long-term memory in *Drosophila*

Short title: Light-dependent memory maintenance in *Drosophila*

Show Inami<sup>1</sup>, Shoma Sato<sup>1</sup>, Shu Kondo<sup>2</sup>, Hiromu Tanimoto<sup>3</sup>, Toshihiro Kitamoto<sup>4,5</sup>, and

Takaomi Sakai<sup>1, \*</sup>

<sup>1</sup>Department of Biological Sciences, Tokyo Metropolitan University, Tokyo 192-0397, Japan

<sup>2</sup>Genetic Strains Research Center, National Institute of Genetics, Shizuoka 411-8540, Japan

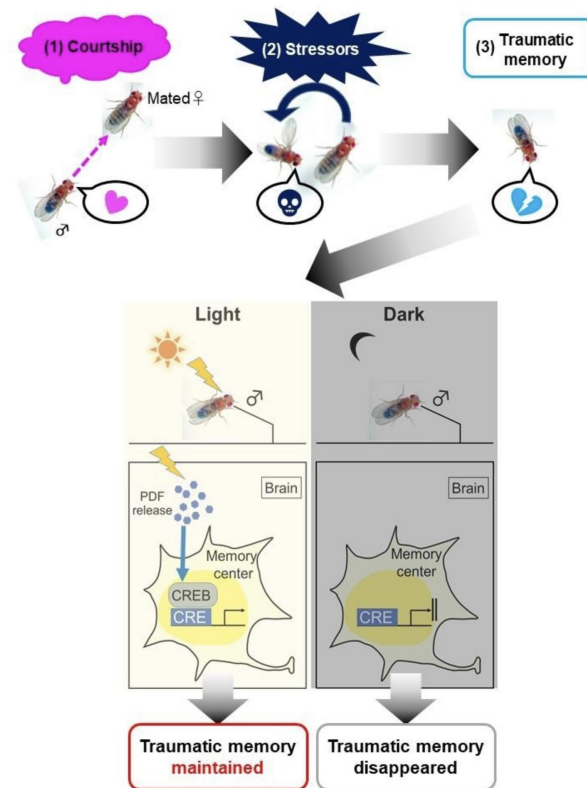
<sup>3</sup>Tohoku University Graduate School of Life Sciences, Sendai 980-8577, Japan

<sup>4</sup>Department of Anesthesia and Pharmacology, Carver College of Medicine, University of Iowa, Iowa City,

IA 52242, USA

<sup>5</sup>Interdisciplinary Programs in Genetics and Neuroscience, University of Iowa, Iowa, Iowa City, IA 52242,

USA



ШНОБЕЛЕВКА:  
ЛУЧШЕЕ ЗА ПАРУ  
ЛЕТ



## SCIENTIFIC REPORTS

OPEN

### In-vivo biomagnetic characterisation of the American cockroach

Ling-Jun Kong<sup>1,2</sup>, Herbert Crepaz<sup>3,4</sup>, Agnieszka Górecka<sup>5,6</sup>, Aleksandra Urbanek<sup>5</sup>, Rainer Dumke<sup>1,3</sup> & Tomasz Paterek<sup>1,3</sup>

We present a quantitative method, utilising a highly sensitive quantum sensor, that extends applicability of magnetorelaxometry to biological samples at physiological temperature. The observed magnetic fields allow for non-invasive determination of physical properties of magnetic materials and their surrounding environment inside the specimen. The method is applied to American cockroaches and reveals magnetic deposits with strikingly different behaviour in alive and dead insects. We discuss consequences of this finding to cockroach magneto-reception. To our knowledge, this work represents the first characterisation of the magnetisation dynamics in live insects and helps to connect results from behavioural experiments on insects in magnetic fields with characterisation of magnetic materials in their corpses.

Many species are capable of perceiving the world through senses inaccessible to humans. Polarisation vision of marine species<sup>1</sup> or magnetic field detection by migratory birds<sup>2</sup> being two well-known examples. Magneto-reception is in fact common to a wide range of organisms, ranging from bacteria to higher vertebrates, and has evolved to a fine-tuned sensory system that may be even takes advantage of quantum coherence<sup>3</sup>. Insights into magneto-reception mechanisms and biomagnetism, magnetic fields that originate in biological systems, not only allow us to understand better different ways of visualising the world but may also find applications in improved man-made sensors inspired by their biological counterparts.

Several behavioural experiments have demonstrated that cockroaches and other insects are capable of magneto-reception, see e.g.<sup>4–17</sup>. Most of the behavioural experiments on cockroaches show their ability to perceive changes of an Earth-strength magnetic field that is rotated with a period of 10 minutes. A different set of experiments found and characterised magnetic particles in insect corpses, see e.g.<sup>18–25</sup>. Naturally one asks if these magnetic particles contribute to magneto-reception. One route to answer this question is to develop techniques for tracking dynamics and quantifying the extent of magnetic materials inside a living insect.

Here we demonstrate a non-invasive method for magnetic field measurements taking advantage of the high precision of atomic magnetometer<sup>26</sup>. It is a form of magnetorelaxometry (MRX)<sup>27</sup> where the magnetic materials to be characterised could be present inside a living organism. The method is applied to study magnetic fields generated by magnetised American cockroaches (*Periplaneta americana*). Our study reveals presence of magnetic materials in their bodies exhibiting distinct magnetic dynamics in alive and dead cockroaches. After magnetisation of alive insects, we observe exponential magnetic field decay to a remnant value, with a decay time of  $50 \pm 28$  minutes. In contradistinction, an average demagnetisation of dead cockroaches displays a much longer decay time of  $47.5 \pm 28.9$  hours.

This clear difference in magnetic field decay is explained by Brownian rotations of magnetic materials in different viscosity environments. Fits of this model to the measured data reveal magnetic particles embedded in an environment which experiences a two orders of magnitude viscosity increment between alive and dead cockroaches. Under the assumption that there were no external magnetic particles on measured insects we find sub-micron sized magnetic deposits and a glassy environment of high viscosity. Such deposits would require

<sup>1</sup>School of Physical and Mathematical Sciences, Nanyang Technological University, Singapore, 637371, Singapore.  
<sup>2</sup>MOE Key Laboratory of Weak Light Nonlinear Photonics and School of Physics, Nankai University, Tianjin, 300071, China.  
<sup>3</sup>Centre for Quantum Technologies, National University of Singapore, Singapore, 117543, Singapore.  
<sup>4</sup>School of Physics and Astronomy, Monash University, Melbourne, 3800, Australia.  
<sup>5</sup>Department of Invertebrate Zoology and Parasitology, University of Gdańsk, Gdańsk, 80-308, Poland.  
Correspondence and requests for materials should be addressed to T.P. (email: tomasz.paterk@ntu.edu.sg)

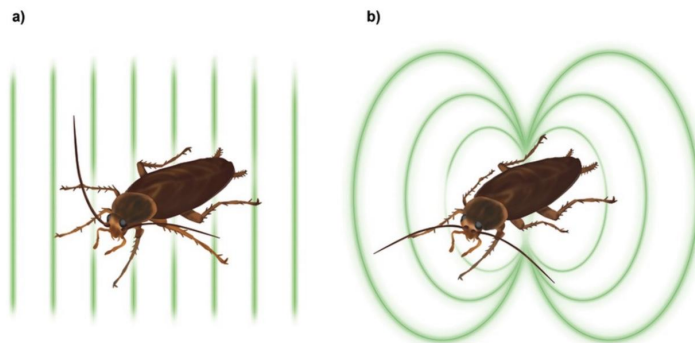


**Figure 1.** Sketch of the experiment. (a) American cockroaches were placed in a strong magnetic field aligned perpendicular to the thorax as illustrated by the green lines. Using an atomic magnetometer we monitored the dynamics of the magnetic field generated by the magnetised insects. (b) The magnetic field is very close to the field of magnetic dipole normal to the thorax. Published with permission from T. Yeo.

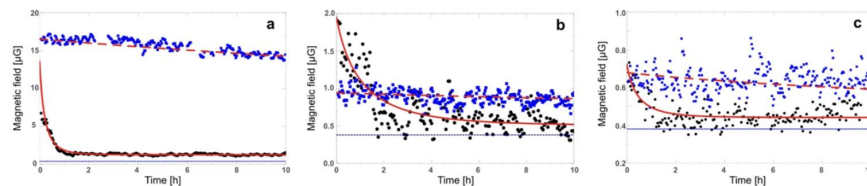


**Figure 2.** Magnetic field decay from magnetised American cockroaches. Black dots show the measured time dependence of the magnetic field for alive cockroaches and blue squares show this dependence for the dead ones. Different panels present exemplary data for different insects. They were chosen to show the typical sets where the initial magnetisation of alive cockroach can be higher, similar or lower than the initial magnetisation of the dead one. This is captured in our model as well. Altogether we conducted 15 measurements lasting longer than 10 hours each and additionally more than 10 shorter measurements. The thick red lines represent simulation of our model, fitting the data: solid for alive cockroaches and dashed for dead ones. The exponential decay time of the magnetic field is (a) 25 mins [82.6 hours], (b) 71 mins [36.3 hours], (c) 30 mins [24 hours] for alive [dead] cockroach. The average exponential decay time over all measurements is  $50 \pm 28$  mins ( $47.5 \pm 28.9$  hours) for alive [dead] cockroaches. The offset magnetisation of  $0.38 \mu\text{G}$  (thin dashed line) is attributed to the cockroach container dominating the signal for unmagnetised cockroaches. Each data-point has an uncertainty of  $0.08 \mu\text{G}$ . Note different vertical scales in different panels.

# 2019. Анатомия. За исследования температурной асимметрии человеческой МОШОНКИ НА ГОЛЫХ И ОДЕТЫХ ПОЧТАЛЬОНАХ

Human Reproduction Vol.22, No.8 pp. 2178–2182, 2007

doi:10.1093/humrep/dem133

## Thermal asymmetry of the human scrotum

---

B. Bengoudifa and R. Mieuisset<sup>1</sup>

*Groupe de Recherche en Fertilité Humaine, Université Toulouse III—Paul Sabatier, EA 3694, Hôpital Paule de Viguier, 330 Avenue de Grande-Bretagne, TSA 70034, Toulouse Cedex 9, France*

<sup>1</sup>Correspondence address. Tel: +33 567 771027; Fax: +33 567 771026; E-mail: mieusset.r@chu-toulouse.fr

**BACKGROUND:** Scrotal temperatures in men have been reported to be either similar on both sides or higher on the left than the right scrotum. We aimed to clarify this discrepancy from new data. **METHODS:** Retrospective analyses of scrotal temperatures in men aged 20–52 years measured every 2 min with probes connected to a data collector in three experiments. In Experiment I, eight men have been submitted to four successive body positions for 15 min each, first naked then clothed. Experiment II involved 11 postal employees working in a standing position for 90 min continuously. Experiment III involved 11 bus drivers and a 90 min period of continuous driving. Outcome parameters were left and right scrotal temperatures. **RESULTS:** In Experiment I, mean values and kinetics of scrotal temperature differed significantly in the naked and clothed state. In all three experiments, left scrotal temperature in the clothed state was higher than right scrotal temperature in terms of mean values and temperature kinetics. **CONCLUSIONS:** Lack of thermal symmetry was seen in the right and left scrotum, whether naked or clothed, and this applied regardless of position or activity when clothed. This thermal difference between right and left scrotum could contribute to the asymmetry in the male external genital organs.

*Keywords:* clothing; genital asymmetry; kinetics; posture; scrotal temperatures

2019. Премия мира за исследование наиболее приятных для чесания  
поверхностей человеческого тела



CLINICAL AND LABORATORY INVESTIGATIONS

# The pleasurability of scratching an itch: a psychophysical and topographical assessment

G.A. bin Saif, A.D.P. Papoiu, L. Banari, F. McGlone, S.G. Kwatra, Y-H. Chan, G. Yosipovitch

First published: 13 January 2012 | <https://doi.org/10.1111/j.1365-2133.2012.10826.x> |

Citations: 22

# 2019. Физика. За доклад о физических причинах кубической формы фекалий у вомбатов

## Bulletin of the American Physical Society

[Bulletin Home](#)[My Scheduler](#)[Epitome](#)[Author Index](#)[Session Index](#)[Invited Speaker](#)[Chair Index](#)[Word Search](#)[Affiliation Search](#)[Using My Scheduler](#)

### 71st Annual Meeting of the APS Division of Fluid Dynamics

Volume 63, Number 13

Sunday–Tuesday, November 18–20, 2018; Atlanta, Georgia

#### **Session E19: Biological fluid dynamics: General I**

5:10 PM–6:28 PM, Sunday, November 18, 2018

Georgia World Congress Center Room: B306

Chair: David Saintillan, University of California, San Diego

Abstract ID: BAPS.2018.DFD.E19.1

#### **Abstract: E19.00001 : How do wombats make cubed poo?**

5:10 PM–5:23 PM

*Abstract* →

#### **Presenter:**

Patricia J Yang  
(Georgia Inst of Tech)

#### **Authors:**

Patricia J Yang  
(Georgia Inst of Tech)

Miles Chan  
(Georgia Inst of Tech)

Scott Carver  
(University of Tasmania, Australia)

David L Hu  
(Georgia Inst of Tech)

Wombats are fossorial herbivorous Australian marsupials with the distinctive feature of producing cubic feces, which is unique in the animal kingdom. In the built world, cubic structures are created by extrusion or injection molding, but there are few examples of this feat in nature. We investigate how wombats produce cubic feces, through investigation of the structure and mechanics of two dissected alimentary systems of wombats—derived from veterinary euthanized individuals following motor vehicle collisions in Tasmania, Australia. In the final 8 percent of the intestine, feces changed from a liquid-like state into a solid state composed of separated cubes of length 2 cm. This shape change was due to the azimuthally varying elastic properties of the intestinal wall. By emptying the intestine and inflating it with a long balloon, we found that the local strain varies from 20 percent at the cube's corners to 75 percent at its edges. Thus, the intestine stretches preferentially at the walls to facilitate cube formation. This study addresses the long-standing mystery of cubic scat formation and provides insight into new manufacturing techniques for non-axisymmetric structures using soft tissues.



# 2018. Медицина.

## За нахождение действенного способа выведения камней из почек при катании на американских горках

From the Doctors Clinic  
in Poulsbo, Washington  
(Dr Mitchell), and the  
Department of Osteopathic  
Surgical Specialties at the  
Michigan State University  
College of Osteopathic  
Medicine in East Lansing  
(Dr Wartinger).


Financial Disclosures:  
None reported.

Support: None reported.

Address correspondence to  
David D. Wartinger, DO, JD,  
1244 Joann Ln,  
Williamston, MI  
48895-9448.

E-mail:  
dave@denaliorganics.com;  
david.wartinger@hc.msu.edu

Submitted  
June 14, 2016;  
revision received  
August 5, 2016;  
accepted  
August 25, 2016.

 Video commentary  
from Dr Wartinger  
is available online.

## Validation of a Functional Pyelocalyceal Renal Model for the Evaluation of Renal Calculi Passage While Riding a Roller Coaster

Marc A. Mitchell, DO  
David D. Wartinger, DO, JD

**Context:** The identification and evaluation of activities capable of dislodging calyceal renal calculi require a patient surrogate or validated functional pyelocalyceal renal model.

**Objective:** To evaluate roller coaster facilitation of calyceal renal calculi passage using a functional pyelocalyceal renal model.

**Methods:** A previously described adult ureteroscopy and renoscopy simulator (Ideal Anatomic) was modified and remolded to function as a patient surrogate. Three renal calculi of different sizes from the patient who provided the original computed tomographic urograph on which the simulator was based were used. The renal calculi were suspended in urine in the model and taken for 20 rides on the Big Thunder Mountain Railroad roller coaster at Walt Disney World in Orlando, Florida. The roller coaster rides were analyzed using variables of renal calculi volume, calyceal location, model position on the roller coaster, and renal calculi passage.

**Results:** Sixty renal calculi rides were analyzed. Independent of renal calculi volume and calyceal location, front seating on the roller coaster resulted in a passage rate of 4 of 24. Independent of renal calculi volume and calyceal location, rear seating on the roller coaster resulted in a passage rate of 23 of 36. Independent of renal calculi volume in rear seating, calyceal location differed in passage rates, with an upper calyceal calculi passage rate of 100%; a middle calyceal passage rate of 55.6%; and a lower calyceal passage rate of 40.0%.

**Conclusion:** The functional pyelocalyceal renal model serves as a functional patient surrogate to evaluate activities that facilitate calyceal renal calculi passage. The rear seating position on the roller coaster led to the most renal calculi passages.

*J Am Osteopath Assoc.* 2016;116(10):647-652  
doi:10.7556/jaoa.2016.128

**Keywords:** calyceal, kidney stone, renal calculi, roller coaster

# 2018. Химия. За изучения свойств человеческой слюны как чистящего средства

## TECHNICAL AND ANALYTICAL NOTES

---

### HUMAN SALIVA AS A CLEANING AGENT FOR DIRTY SURFACES

Paula M. S. Romão, Adília M. Alarcão and César A. N. Viana

**Abstract**—The use of human saliva to clean dirty surfaces has been an intuitive practice for many generations. The authors have established the scientific basis for this practice by means of qualitative tests and chromatographic techniques.  $\alpha$ -amylase was found to be the main constituent responsible for the cleaning power of saliva and therefore amylasic preparations obtained from bread or from micro-organisms were tested as saliva substitutes.

#### 1 Introduction

Saliva has long been widely used as a cleaning agent for all kinds of surfaces and has shown good performance, especially on gold-leaf objects [1, 2]. At the Instituto José de Figueiredo (Lisbon, Portugal) it was noticed that some conservators preferred their own saliva to any other solvent for cleaning fragile painted layers on

#### 2.2 Ion-exchange chromatography

Saliva was collected with a plastic syringe and subjected to refrigerated ( $T = 4^{\circ}\text{C}$ ) centrifuging (10,000g, 50 minutes), and the supernatant was dialyzed against NaCl. 6ml of this solution were applied to a carboxymethylcellulose (MCM, Sigma, pre-swollen,  $1\text{meq g}^{-1}$ ) column ( $0.7 \times 10\text{cm}$ ) previously equilibrated in 5mM disodium phosphate and 1mM acetic acid, pH 5.9 [4]. The elute was made up with 0.1M sodium chloride (rate =  $10\text{ml h}^{-1}$ ) and each fraction of 3.8ml was analyzed for protein ( $\text{OD}_{280}$ ) and amylase activity [3, 4].

#### 2.3 Testing the enzymatic fractions

The solubility and resistance tests described above were carried out with the enzymatic fractions obtained by ion-exchange

# 2018. Здоровое питание. За изучения питательной ценности человеческого тела и оценку полноценности диеты при каннибализме

www.nature.com/scientificreports

## SCIENTIFIC REPORTS

OPEN

### Assessing the calorific significance of episodes of human cannibalism in the Palaeolithic

James Cole

Received: 11 October 2016  
Accepted: 13 February 2017  
Published: 06 April 2017

Episodes of Palaeolithic cannibalism have frequently been defined as 'nutritional' in nature, but with little empirical evidence to assess their dietary significance. This paper presents a nutritional template that offers a proxy calorie value for the human body. When applied to the Palaeolithic record, the template provides a framework for assessing the dietary value of prehistoric cannibalistic episodes compared to the faunal record. Results show that humans have a comparable nutritional value to those faunal species that match our typical body weight, but significantly lower than a range of fauna often found in association with anthropogenically modified hominin remains. This could suggest that the motivations behind hominin *anthropophagy* may not have been purely nutritionally motivated. It is proposed here that the comparatively low nutritional value of hominin cannibalism episodes support more socially or culturally driven narratives in the interpretation of Palaeolithic cannibalism.

Human cannibalism is a subject that continues to hold a morbid fascination within modern societies. In particular, identifying the motivations for human cannibalism remains a contentious issue. In modern humans, the motivations for cannibalism have been related to any combination of the following: survival; psychotic or criminal; aggressive; spiritual or ritual; gastronomic or dietary; and medicinal<sup>1–4</sup>. All of these can be further categorised as inter (exo-) and intra-group (endo-) cannibalism, with differing motivational states depending on whether or not the consumed is a member of the consumer's immediate social network<sup>4,5</sup>. Cannibalism is not, however, purely a characteristic of modern humans, and has been practiced by a range of hominin species from at least the early Pleistocene<sup>6</sup>. The evidence from the archaeological record would suggest that, whilst different hominin species clearly had the capacity for cannibalistic practices, not every hominin population did so, on the basis that not all hominin remains show evidence for anthropogenic modifications. The hominin remains that do exhibit anthropogenic modifications may imply they were cannibalised, although, there are also alternate explanations such as defleshing and exhumation.

Globally, the number of Palaeolithic cannibalism fossil sites remain relatively few<sup>7</sup>, further supporting the notion that the practice of hominin cannibalism may have been an exceptional activity. However, given the sparse nature of the hominin fossil record, the fact that we have evidence for cannibalism at all infers that the behaviour was perhaps more common within prehistoric populations than the number of archaeological sites suggests. Additional support for the possible widespread nature of prehistoric cannibalism comes from genetic studies of global patterns of transmissible spongiform encephalopathies (TSEs)<sup>8</sup>, which imply that prehistoric TSE polymorphisms were a routine feature of hominin life. Mead *et al.*, for example, propose that the repeated exposure of hominins to the effects of TSEs (such as Kuru and Creutzfeldt-Jakob disease) resulting from cannibalistic activities, drove the polymorphism adaptation as a selective advantage within prehistoric populations<sup>9</sup>. These authors argue that such an adaptation would only be necessary if exposure to the neurodegenerative diseases (through the consumption of infected flesh) was a common feature in prehistoric hominin lifeways.

Our understanding of prehistoric cannibalism has increased exponentially over the last few years thanks to methodological advances and increasing interpretive rigour when examining and recognising anthropogenically modified hominin remains<sup>10–12</sup>. In the majority of studies, the interpretation is that cannibalism was practiced for nutritional reasons<sup>2,5,6,13</sup> although there has never been a way to quantify how nutritional these episodes may be. For example, while varied practices of consumption have been identified amongst Neanderthal populations from Moulou-Guercy (France)<sup>14</sup>, Cueva del Sidrón (Spain)<sup>15</sup>, Cueva del Boquete de Zafarraya (Spain)<sup>16</sup>, Padrelles (France)<sup>17,18</sup>, and Troisième caverne de Goyet (Belgium)<sup>19</sup>, all are broadly interpreted as nutritional. A small

Body Component	Average Weight (kg)	Nutritional Value in Calories (Fat + Protein)
Skeletal Muscle [total]:	[24.90]	[32375.50]
*Torso and Head	4.17	5418.67
*Upper arms	5.73	7451.16
*Forearms	1.28	1664.48
*Thighs	10.27	13354.88
*Calves	3.45	4486.30
*Brain, Spinal Cord, Nerve Trunks	1.69	2706.00
*Lungs	2.06	1596.50
*Heart	0.44	650.75
*Kidneys	0.35	376.00
*Liver	1.88	2569.50
*Adipose Tissue	8.72	49938.50
*Skin	4.91	10278.00
*Skeleton	10.31	25331.50
Teeth	0.04	36.00
Nerve Tissue	1.53	2001.00
Alimentary tract	1.23	1263.25
Spleen	0.15	128.33
Pancreas	0.09	160.50
Remaining Tissue: Liquid	1.03	469.50
Solid	6.66	13890.50
Total	65.99	143771.33
Total*	55.26	125822.25

**Table 1. Average weight and calorific values for parts of the human body.** \*Parts of the human body reasonably assumed to have been consumed on a regular interval based on ethnographic<sup>4,45</sup> and archaeological sources (see Table 3).

	Male adult (18+ years)	Male adolescent (11–18 years)	Male juvenile (7–11 years)	Male child (4–7 years)	Male infant (0–4 years)
Average Weight (kg)	65.99 <sup>a</sup>	50.31 <sup>b</sup>	28.74 <sup>b</sup>	19.85 <sup>b</sup>	13.52 <sup>c</sup>
% of Adult weight	100.00	76.23	43.55	30.08	20.48
Calorie value total body	143771.33 <sup>d</sup>	109596.88	62612.41	32966.74	12823.02
Calorie value* estimates from Table 1	125822.25 <sup>d</sup>	95914.30	41770.68	12564.62	2573.23
Calorie value skeletal muscle	32375.50 <sup>d</sup>	24679.84	10748.07	3233.02	662.12

**Table 2. Estimated total calorific values for male adults, adolescents, juveniles and infants.** <sup>a</sup>Average value used in this study from sample (S1) – 18+ weight from <sup>b</sup>is 67 kg and thought to be comparable with the average weight from this study (65.99 kg), therefore no corrections were necessary. <sup>b</sup>Values obtained from<sup>17</sup> based on average weights per age (4–18) on the 50<sup>th</sup> centile line. <sup>c</sup>Values obtained from<sup>16</sup> based on average weights per age (0–4) on the 50<sup>th</sup> centile line. <sup>d</sup>Calorie values from Table 1.

School of Environment and Technology, University of Brighton, Cockcroft Building, Lewes Road Brighton, BN2 4GJ, UK. Correspondence and requests for materials should be addressed to J.C. (email: J.N.Cole@brighton.ac.uk)